Optical characterisation of hybrid antireflective coatings using spectrophotometric and ellipsometric measurements

V. Janicki, J. Sancho-Parramon, O. Stenzel, M. Lappschies, B. Görtz, C. Rickers, C. Polenzky and U. Richter

V. Janicki and J. Sancho-Parramon are with the Ruđer Bošković Institute, Bijenička 54, 10000 Zagreb, Croatia. O. Stenzel is with the Fraunhofer Institut für Angewandte Optik und Feinmechanik, Albert Einstein Strasse 7, 07745 Jena, Germany. M. Lappschies and B. Görtz are with the Laser Zentrum Hannover, Hollerithallee 8, 30419 Hannover, Germany. C. Rickers and C. Polenzky are with the Fraunhofer Institut für Schicht- und Oberflächentechnik, Bienroder Weg 54 E, 38108 Braunschweig, Germany. U. Richter is with SENTECH Instruments GmbH, Carl-Scheele-Strasse 16, 12489 Berlin, Germany.

A hybrid antireflective coating combining homogeneous layers and linear gradient refractive index layers has been deposited using different techniques. The samples were analysed optically based on spectrophotometric and spectroscopic ellipsometry measurements under different angles of incidence in order to precisely characterise the coatings. The Lorentz-Lorenz model has been used for calculation of refractive index of material mixtures in gradient and constant index layers of the coating. The obtained refractive index profiles have been compared with the targeted ones to detect errors in processes of deposition.

Key words: *antireflective coating, optical characterisation, hybrid coating, reverse engineering, variable angle spectroscopic ellipsometry.*

OCIS codes: 310.1210, 310.3840

1. Introduction

Optical characterisation methods are of utmost importance in analysis of coatings in thin films science and technology. They allow determination of refractive index, thickness of the coating and variation of refractive index through the depth of the coating (i.e. inhomogeneity). Numerous methods for optical characterisation of thin films have been developed. These methods usually start from modelling the optical behaviour of the sample through a set of parameters which represents some kind of initial approximation. The optimal values of these parameters are found by the minimisation of a merit function that quantifies the agreement between experimental measurements and the data simulated from the sample model. The optimisation procedure is normally carried out using numerical techniques. Some of these methods are based on analysis of spectrophotometric measurements[1], i. e. reflectance ($R(\lambda)$) and transmittance ($T(\lambda)$) as function of the wavelength (λ) in a certain spectral range, and some on analysis of ellipsometric Δ and Ψ functions[2,3] or their combination[4,5,6]. Spectroscopic ellipsometry has been shown to be a very sensitive technique with respect to the variation of the refractive index with the layer thickness[7]. A typical problem of these methods is the multiplicity of solutions, that is, the existence of different combination of parameters values that minimise the merit function. In order to avoid this problem it is useful to have more measurements of the same sample, like measurements

taken at different angles of incidence, to combine spectrophotometry and spectroscopic ellipsometry, or to include non-optical characterization methods[8]. This leads to a significant reduction of the solution multiplicity, thus facilitating the selection of the physically meaningful one.

The model, i.e. the refractive index profile found by optical characterisation, can be compared with the targeted profile that was aimed to be deposited. Analysis of the differences between the two is crucial in detecting the errors in the process of deposition and improving the manufacturing procedures.

In this work, optical characterization methods are applied to the study of hybrid antireflective coatings. The coatings were designed to minimise the reflectance of a BK7 glass substrate in the wavelength range 480-680 nm in the range of 0°-50° of angle of incidence[9]. The hybrid coatings combine refractive index gradients (ramps) with layers of constant refractive index through the thickness of the film. The obtained hybrid design was refined according to the materials available for the different deposition techniques, and subsequently, a round-robin experiment of deposition with different techniques has been performed[10]. The studied samples were deposited by electron beam evaporation (EBE), radio frequency magnetron-sputtering (RFS) and ion beam sputtering (IBS). In all three techniques SiO_2 was used as the low index material, while high index materials were Nb_2O_5, Ta_2O_5 and TiO_2, respectively. In the case of IBS coatings, ramps are approximated and deposited as sequence of ultrathin layers with constant refractive indices.

Spectrophotometric and ellipsometric measurements under different angles of incidence were performed for optical characterisation of samples. The refractive index profiles thus

obtained were compared with the targeted ones and conclusions about errors in the deposition processes and suggestions how to minimize them were proposed.

2. Optical characterisation and numerical data evaluation

Due to the desired optical properties, there are no significant fringes with considerable amplitude in the structure of the spectra of hybrid AR coating in the visible range. On the contrary, reflectance and transmittance is rather constant in most of the spectral range of interest. Reflectance and transmittance measurements were combined with ellipsometric measurements. Spectrophotometric measurements were performed with a Perkin Elmer Lambda 900 spectrophotometer. A VN-attachment allowing absolute measurement of reflectance without moving the sample after the transmittance measurement has been used. Reflectance and transmittance in the spectral range 400-850 nm were measured in steps of 2 nm: R and T measured at angle of incidence of 6 degrees and R_s, R_p, T_s and T_p at 45 degrees. Measurements of spectra of ellipsometric Δ and Ψ functions were performed with a standard SENTECH SE800 ellipsometer with microspot (200 μm). Usage of microspot, together with thickness of the glass (2mm) results in measurements without the contribution of reflection from the back side of the substrate. Ellipsometric measurements in the same spectral range as R and T were taken at the angles of 50, 55 and 60 degrees, at 575 wavelength points per angle. These angles were chosen for the ellipsometric functions to present maximum amplitude of their interferential fringes. In the optimisation process $\cos\Delta$ and $\cos 2\Psi$ were considered. The bare substrates were characterised previously, by means of spectrophotometry.

For the optical characterisation of the samples we used general-purpose software[11] that allows determination of the optimal value of a set of parameters defining the sample by fitting experimental spectra. Each sample has been represented as an in-depth inhomogeneous coating

deposited onto a substrate with known optical constants. According to the design, some parts of the coating have a constant composition making constant refractive index layers, while others show a linear variation in composition, corresponding to the ramps in the design. The inhomogeneity of a ramp is taken into account by dividing it into a given number of homogeneous sublayers, all with the same thickness. Each homogeneous layer and sublayer has been modelled as a mixture of the two materials of high (n_H) and low refractive index (n_L) with volume fractions f_H and f_L, being $f_H + f_L$=1. For each sublayer the volume fraction of the high index material is given by:

$$f_{H-i} = f_{H-start} + \frac{f_{H-end} - f_{H-start}}{N_{sublayer}}\left(i - \frac{1}{2}\right). \quad (1)$$

Here f_{H-i} is the volume fraction of the material of high refractive index in the sublayer i (i = 1, 2, 3, ... N_{sub}), $f_{H-start}$ and f_{H-end} are the values of the volume fractions of high index material at the beginning and at the end of the ramp and $N_{sublayer}$ is the number of sublayers. The optical constants for each mixture layer can be calculated using different mixing formula: Bruggeman[12], Lorentz-Lorenz[13], Maxwell Garnett[14] or a linear combination of refractive indices[15]. It has been suggested[16] that an appropriate description of the optical constants of the mixture in our case is given by the Lorentz-Lorenz formula:

$$\frac{\varepsilon_{eff} - 1}{\varepsilon_{eff} + 2} = f_L \frac{\varepsilon_L - 1}{\varepsilon_L + 2} + f_H \frac{\varepsilon_H - 1}{\varepsilon_H + 2} \quad (2)$$

where ε_{eff}, ε_H and ε_L are the effective dielectric functions of the mixture and the high and low index material, respectively. The optical constants of the high and low index materials can be used either from a data file or represented with a dispersion model.

In this way the sample is represented through a limited set of parameters: volume fraction and thickness for each layer and parameters defining the dispersion model for each material. The

software enables fixing these parameters to a given value or to optimize them within some limits. Furthermore, it is possible to establish links between different parameters by imposing the continuity of the volume fraction at the interface of different layers. The optimisation of the parameters is carried out by the minimisation of a merit function that is the chi-square estimator χ^2:

$$\chi^2 = \frac{1}{N-m-1}\sum_{j=1}^{N_s}\sum_{k=1}^{N_j}\left(\frac{y_k^j - y^j\left(x_k; P_1, \cdots, P_m\right)}{\sigma_k^j}\right)^2 \tag{3}$$

where N is the total number of experimental data points, N_s is the number of measured spectra, each one containing N_j experimental data points, y_k^j represents measured values at the wavelength x_k with associated experimental error σ_k^j , $y_j(x_k;P_1,..., P_m)$ is the corresponding value calculated using standard thin film computation algorithms[17] and P_1, …, P_m are the m parameters being optimized. It must be highlighted that this merit function permits considering different magnitudes simultaneously in the same optimisation procedure (like spectrophotometric and ellipsometric measurements) since the quantities being added are dimensionless. The minimisation of the merit function is carried out using the Downhill-Simplex algorithm[18].

Upon optimization is possible to evaluate the statistical uncertainties of the parameters. Uncertainties give estimation how precisely the parameters are determined according to experimental error of the used data. These uncertainties are given as confidence limits[18] that define a region in the parameter space which contains a certain percentage of the total probability distribution of the parameter, i.e. that there exists certain probability that the true value of the parameter is within this region. The uncertainties of the parameters (δP_i) are calculated as:

$$\delta P_i = \sqrt{\Delta\chi^2}\sqrt{C_{ii}}\ , \tag{4}$$

where $\Delta\chi^2$ defines the confidence region (we have chosen $\Delta\chi^2$=2.70 corresponding to 90% probability for the confidence region) and C_{ii} is diagonal element of the inverse of the curvature matrix α, with elements given by

$$\alpha_{ij} = (N - m - 1)\frac{\partial^2 \chi^2}{\partial P_i \partial P_j}. \quad (5)$$

Thus, the curvature matrix is the matrix of the second derivatives of the merit function in respect to the parameters that are optimised. This matrix is numerically evaluated at the minimum of the merit function.

The original targeted designs have been taken as starting designs for optical characterisation defining the initial values of the parameters to be optimised. Each ramp in EBE and RFS sample was divided into 8 sublayers. In this way, only starting and ending volume fractions of one material, as well as the thickness of the ramp, were optimized. Initially, at the beginning of optimization procedure, thickness limits of RFS and IBS samples were set to 3% and of EBE to 6% of the design's thickness, that correspond to the estimated deviation in thickness for each technique of deposition[10]. In the case of EBE sample, higher errors are expected due to the fact that rates of deposition were controlled by quartz monitor only, because of high deposition rates compared with the other two techniques and because of instabilities of these rates[8] due to the nonuniform evaporation of the materials from the rotating crucible. Refractive indices of the pure materials (pure, in the sense that they were not mixtures of materials prepared in a process of co-deposition) obtained from the measurements of the single material layers were used. In the next step, in order to improve the data fits, the optimisation of the optical constants of the materials by using dispersion formulas was allowed. For the case of the RFS sample, spectrophotometric measurements indicated the presence of absorption (R+T<1). Since in RFS high index material data file absorption was neglected, it was included in

optimisation by a dispersion formula for the extinction coefficient. Finally, the effect of removing the thickness limits of individual layers (one at the time) to improvement of quality of the fit was studied.

3. Results and discussion

The optimized models of refractive index profiles that are obtained in the process of optical characterisation, together with the original designs that were used as starting models, are shown in Fig. 1 for all three samples. In Table 1 numerical values of the materials Cauchy parameters and refractive indices are presented. The spectral characteristics of the models, compared with the measured and design spectra, are given in Fig. 2, 3 and 4. Figure parts (a) and (b) present R and T measurements, respectively, shown in the scale 0-1. Ellipsometric functions $\cos\Delta$ and $\cos 2\Psi$ are presented in figure parts (c) and (d).

Tables 2, 3, and 4 show the comparison of designs and models, in the sense of discrepancies of thicknesses and refractive indices. Errors are calculated as the absolute value of the difference of the parameter value in the model and design, divided by the parameter value in the design. The errors are given in percents.

Generally speaking, the characterisation procedure led to a remarkable agreement between the simulated and experimental data and a model close (i.e. within the expected errors) to the initial design. Differences between the obtained model and the initial design can be explained in terms of deviations in the deposition process. When only spectrophotometric measurements are used for optical characterization, R and T fits of the similar quality are obtained, but with other refractive index profiles which are not consistent with the ellipsometry data. Besides, by adding ellipsometric measurements uncertainties of parameters decrease two to

four times. In accordance, the calculated curvature matrix presents higher values, what implies that minimum of merit function is narrower in comparison when only spectrophotometric measurements are used, that evidences higher stability of solution. In this way, the complementary use of ellipsometric data results in a more realistic model.

The optimisation of the refractive indices of SiO_2 of EBE and RFS samples, modelled with the Cauchy dispersion formula, enabled significant improvement of function of merit. On the contrary, no improvement was achieved by optimising the dispersion parameters of high index materials (except the need to include absorption in Ta_2O_5 of RFS as described above) or SiO_2 of IBS, regardless the used dispersion model. The differences to the data file refractive indices of EBE and RFS samples determined from samples with single layer of silica are between 1% and 2%, the higher corresponding to the RFS sample. Such discrepancy could be explained by different conditions during the process of deposition (pressure or temperature of the substrate) or difference in growth of the material when it is deposited directly to the bare substrate or to the pre-evaporated coating. Besides, for the RFS sample a more probable explanation could be contamination with the high index material. In fact, the found difference in SiO_2 refractive index would correspond to 5% volume fraction of Ta_2O_5 inclusions. The origin of these inclusions could be that SiO_2 target becomes contaminated by Ta_2O_5 while the latter is sputtered. Another possible reason could be as follows: all of the time during the deposition both sources must be kept running. So, at pure material deposition the other source is still running, although at extremely low power. This low power mode can be instable, depending of the process history. It should be possible to avoid this effect by running only one source for pure materials switching the other one off completely and protecting it from contamination with a closed shutter. It can also be reduced by using higher low-power limits. The refractive index

of the layer that was supposed to be pure silica in the model for IBS sample is higher than could be expected for this material (Table 4). The reason for this, similar as for the case of SiO_2 of RFS, could be inclusions of TiO_2. The obtained refractive index of this layer corresponds to silica with 4% of volume fraction of titania. For co-deposition with the IBS technique a specially prepared zone target has been used[19]. The mismatch in dependency of the refractive indices against the target position, leading to co-sputtering of both materials instead of only one of them, can originate from a slightly broadened ion beam[20]. An additional effect may arise from the contamination of the non-sputtered side of the target with the actual coating material. Optical characterization points out that higher than expected refractive indices of SiO_2 layers are crucial issues. Above suggested possible origins of these discrepancies must be checked in order to improve the process.

Regarding thicknesses, they remain within the expected errors of 6% for EBE and 3% for RFS and IBS. Only the third ramp of EBE model and the second one together with Ta_2O_5 layer of RFS model are out of these error ranges, improving the fits significantly. From the Fig. 1(a) it can be seen that the model of EBE sample gives ramps ending with higher refractive index compared to the design. This indicates that the rate of deposition of Nb_2O_5 was higher than expected, i.e. it was not well calibrated. On the contrary, the thickness of the Nb_2O_5 layer is as expected because it was controlled by quartz crystal monitor and not by time of deposition as in the case of ramps. In the case of RFS it is possible that, due to the specific conditions during co-sputtering process mentioned before, the rate of deposition of Ta_2O_5 that was determined from samples coated with pure material and not in the process of co-deposition, is not repeatable in the process of co-deposition, or it suffers from larger deviations which resulted in the error in the thickness of the Ta_2O_5 layer. The true origin of so high thickness error is under study.

It must be highlighted that the characterization started from the simplest model and limited parameters. New parameters (coefficients of dispersion formulas and extinction) were gradually introduced only when trials would confirm it was the only way for significant reduction of merit function that otherwise would remain high. The same applies for increasing limits to some parameters, such as thickness of layer D in EBE model or Ta_2O_5 layer in RFS model. Also, the starting designs were modified within the expected limits and subjected to optimization. The optimization would stop either in merit function significantly higher or very close to the one of the reported optimized model, the later always giving refractive index profile within the given parameter uncertainties and only slightly different from the reported one .

Finally, it must be mentioned that other effective medium theories were tested to describe the optical constants of mixtures. Thus, using Bruggeman formula, merit functions were about 50% higher than those obtained by Lorentz-Lorenz. Indeed, the previous results for TiO_2-SiO_2 mixtures have shown appropriateness of Lorentz-Lorenz model for this type of mixtures[23]. The first results of structural analysis of Nb_2O_5-SiO_2 mixtures indicate the same. However, this will be published elsewhere.

4. Conclusions

Optical characterisation has been successfully applied for the analysis of hybrid antireflective coatings. It has been shown that the combination of spectrophotometric and ellipsometric measurements at different angles of incidence is a proper choice for the characterisation of systems like antireflective coatings, where the optical performance lacks details (fringes) in the reflected and transmitted spectra. The hybrid designs consisting of ramps of refractive index variation through depth of the film and layers of constant refractive index have been represented

with appropriate models. The models had optimisation parameters which number and range were maximally controlled in the process of optimisation. Thus, simple and as realistic solutions as possible were obtained. For calculations of refractive indices of mixture materials the Lorentz-Lorenz model, as the most appropriate one, has been used.

The resulting models were shown to be helpful for determining the possible errors in deposition processes of each of the utilised deposition techniques, and this was the main goal. Thus, it has been found that the thicknesses of the coatings were controlled mainly within the expected accuracy. The main problem in deposition of the studied samples seems to be control of the desired refractive index that could be achieved by means of better determination of deposition rate of high index material. The results of optical characterization indicate higher than expected refractive index of pure low index material layers that could be explained by contamination of the coating. Therefore, origins of possible undesired co-deposition or contamination should be investigated in order to improve the deposition processes.

Acknowledgements

The authors thank the German Federal Ministry of Economics and Labour (BMWA) for the financial support within research project “Rugate Filters”. Vesna Janicki wishes to thank the Fraunhofer Society in Germany for a Fraunhofer Fellowship at Institut für Angewandte Optik und Feinmechanik in Jena. The authors thank Heidi Haase for technical assistance.

References

1. A. Piegari, G. Emilliani, “Analysis of inhomogeneous thin films by spectrophotometric measurements”, Thin Solid Films **171**, 243-250 (1989).

2. G. Parjadis de Lariviere, J.M. Frigerio, J. Rivory, F. Abeles, “Estimate of the degree of inhomogeneity of the refractive index of dielectric films from spectroscopic ellipsometry”, Appl. Opt. **31**, 6056-6061 (1992).
3. P. Chindaudom, K. Vedam, “Characterization of inhomogeneous transparent substrates by spectroscopic ellipsometry: refractive indices *n(λ)* of some fluoride-coating materials”, Appl. Opt. **33**, 2664-2671 (1994).
4. V. Janicki, H. Zorc, “Refractive index profiling of CeO_2 thin films using reverse engineering methods”, Thin Solid Films **413**, 198-202 (2002).
5. D. Franta, I. Ohlidal, D. Munzar, J. Hora, K. Navratil, C. Manfredotti, F. Fizzotti, E. Vittone, “Complete optical characterization of imperfect hydrogenated amorphous silicon Layers by spectroscopic ellipsometry and spectroscopic reflectometry”, Thin Solid Films **343-344**, 295-298 (1999).
6. D. Franta, I. Ohlidal, “Optical characterization of inhomogeneous thin films of ZrO_2 by spectroscopic ellipsometry and spectroscopic reflectometry”, Surf. Interface Anal. **30**, 574-579 (2000).
7. K. Vedam, P. J. McMarr, J. Narayan, “Non destructive depth profiling by spectroscopic ellipsometry”, Appl. Phys. Lett. 47, 339-341, (1985).
8. R. Leitel, O. Stenzel, S. Wilbrandt, D. . Gäbler, V. Janicki, N. Kaiser, “Optical and non-optical characterization of Nb_2O_5-SiO_2 compositional graded-index layers and rugate structures”, Thin Solid Films **497**, 135-141 (2006).
9. V. Janicki, S. Wilbrandt, O. Stenzel, D. Gäbler, N. Kaiser, A. Tikhonravov, M. Trubetskov, T. Amotchkina, “Hybrid optical coating design for omnidirectional antireflection purposes”, J. Opt. A: Pure Appl. Opt. **7**, L9-L12 (2005).

10. V. Janicki, D. Gäbler, S. Wilbrandt, R. Leitel, O. Stenzel, N. Kaiser, M. Lappschies, B. Görtz, D. Ristau, C. Rickers, M. Vergöhl, “Deposition and spectral performance of an inhomogeneous wide-angular antireflective coating”, Appl. Opt. **45**, 7851-7857 (2006).
11. S. Bosch, J. Ferré-Borrull, J. Sancho-Parramon, “A general-purpose software for the optical characterization of thin films: specific features for microelectronic applications”, Solid State Electron. 45, (703-709), (2001).
12. D. A. Bruggeman, “Berechnung verschiedener physikalischer Konstanten von heterogenen Substanzen“, Ann. Phys. 24, 636-679, (1935).
13. L. Lorenz, “Über die Refractionsconstante,” Ann. Phys. 11, 70-103 (1880).
14. J. C. Maxwell Garnett, “Colors in metal glasses and metallic films”, Philos. T. Roy. Soc. A, 203, 385-420, (1904).
15. A. V. Tikhonravov, M. K. Trubetskov, T. V. Amotchkina, M. A. Kokarev, N. Kaiser, O. Stenzel, S. Wilbrandt, and D. Gäbler, "New optimisation algorithm for the synthesis of rugate optical coatings," Appl. Opt. **45**, 1515-1524 (2006).
16. X. Wang, H. Masumoto, Y. Someno, T. Hirai, “Microstructure and optical properties of amorphous TiO_2-SiO_2 composite films synthesized by helicon plasma sputtering“, Thin Solid Films, **338**, 105-109 (1999).
17. H. Berning, “Physics of thin films”, Vol. 1, 69-121, New York, Academic Press, 1963.
18. W. H. Press, S. A. Teukolsky, W. T. Vetterling, B. P. Flannery “Numerical Recipes in C”, Cambridge University Press, New York, 1992.
19. M. Lappschies, B. Görtz, D. Ristau: “Application of optical broadband monitoring to quasi-rugate filters by ion beam sputtering”, Appl. Opt. **45**, 1502-1506 (2006).

20. M. Lappschies, B. Görtz, D. Ristau: “Optical monitoring of rugate filters”, Proc. SPIE 5963, pp.1Z-1 (2005).

List of table captions

Tab. 1: The dispersion formula for the refractive index was $n(\lambda)=a_0+a_1/\lambda^2$ and for the extinction coefficient $k(\lambda)=k_0 \cdot \exp(k_1/\lambda)$.

Tab.2. Refractive indices correspond to the starting refractive index of the layers. Only the thickness d_{model} of the third ramp (D) is more than 6% higher than the thickness of the original design d_{design}. Average error in refractive index is 2.7%. Error of Nb_2O_5 refractive index is 0 because it was fixed. When allowed to optimize, the quality of the fit did not improve.

Tab.3. Refractive indices correspond to the starting refractive index of the layers. The thickness of the second ramp B d_{model} is 8% higher than the thickness of the original design d_{design} and the thickness of the Ta_2O_5 layer is 27% higher (11 nm). Thicknesses of the other layers are within 3% of error to the starting thickness. Average error in refractive index is 2.2%. Error of Ta_2O_5 refractive index is 0 because it was fixed. When allowed to optimize, the quality of the fit did not improve.

Tab.4. Thickness of each layer is within 3% of error. Thicknesses of 10 layers have reached their minimum/maximum allowed value. There was no improvement to the fit when absorption was introduced. Average error in refractive index is 1.1%.

List of figure captions

Fig 1. The optimized models of refractive index profiles and the original designs that were used as starting models.

Fig. 2. The spectral characteristics of the models compared with the measured spectra of the sample deposited by electron beam evaporation. Spectra of the design have been added for comparison. The back side of the substrate remained uncoated.

Fig. 3. The spectral characteristics of the models compared with the measured spectra of the sample deposited by radio-frequency sputtering. Spectra of the design have been added for comparison. The back side of the substrate remained uncoated.

Fig. 4. The spectral characteristics of the models compared with the measured spectra of the sample deposited ion beam sputtering. Spectra of the design have been added for comparison. The back side of the substrate remained uncoated.

Table 1. Dispersion parameters and material refractive indices

material	a0	a1(nm^2)	k0	k1(nm)	n(570nm)	k(570nm)
Nb_2O_5	data file determined from single layer				2.2838	0
Ta_2O_5	data file determined from single layer		0.00093	0.013	2.1249	9.3e-4 ±0.9e-4
TiO_2	data file determined from single layer				2.4078	0
SiO_2 EBE	1.4703	2790	0	0	1.4789 ±0.0009	0
SiO_2 RFS	1.4852	3520	0	0	1.496 ±0.001	0
SiO_2 IBS	data file determined from single layer				1.4992	0

Table 2. EBE discrepancies from the design (err_d, err_n)

layer	d_{design} (nm)	d_{model} (nm)	err_d (%)	n_{design} at 570nm	n_{model} at 570nm	err_n (%) at 570nm
A	124.05	118.68±0.16	4.33	1.5980	1.6153±0.0014	1.07
B	112.89	106.2±0.4	5.95	2.1110	2.236±0.003	6.00
C	35.91	34±4	6.00	1.5980	1.595±0.002	0.21
D	87.15	96.7±1.0	10.98	2.1110	2.273±0.011	7.67
E (Nb_2O_5)	75.46	72.9±1.1	3.38	2.2840	2.2840	0.00
F (SiO_2)	95.55	101.00±0.06	5.70	1.4630	1.4789±0.0009	1.06

Table 3. RFS discrepancies from the design (err_d, err_n)

layer	d_{design} (nm)	d_{model} (nm)	err_d (%)	n_{design} at 570nm	n_{model} at 570nm	err_n (%) at 570nm
A	129.72	126.97±0.08	2.12	1.6000	1.6568±0.0007	3.55
B	90.05	97.3±0.4	8.03	2.1250	2.125±0.002	0.00
C	76.97	76±4	1.51	1.6000	1.594±0.002	0.21
D	96.39	96.4±0.6	0.04	1.6000	1.594±0.002	0.21
E (Ta_2O_5)	41.44	52.7±0.4	27.08	2.1250	2.1250	0.00
F (SiO_2)	97.45	97.50±0.09	0.06	1.4690	1.496±0.001	1.84

Table 4. IBS discrepancies from the design (err_d, err_n)

layer	d_{design} (nm)	d_{model} (nm)	err_d (%)	n_{design} at 570nm	n_{model} at 570nm	err_n (%) at 570nm
A1	31.84	32.7±0.7	2.61	1.5997	1.5857±0.0002	0.90
A2	8.61	8.8±0.7	2.21	1.6715	1.6631±0.0005	0.49
A3	10.61	10.82±0.15	1.98	1.7421	1.7709±0.0017	1.65
A4	13.90	14.32±0.13	3.00	1.8144	1.838±0.003	1.34
A5	17.22	17.74±0.14	3.00	1.8849	1.889±0.004	0.26
A6	18.27	18.71±0.12	2.41	1.9570	1.934±0.004	1.16
A7	16.29	15.8±0.6	3.00	2.0276	2.019±0.005	0.42
B1	34.72	35.8±0.4	3.00	2.1005	2.126±0.003	1.21
B2	13.57	13.84±0.18	1.99	2.0367	2.0466±0.0009	0.47
B3	13.70	13.3±0.9	3.00	1.9752	1.961±0.004	0.76
B4	13.34	13.7±0.5	3.00	1.9122	1.914±0.002	0.09
B5	12.12	12.25±0.17	1.07	1.8496	1.8788±0.0011	1.60
B6	8.94	9.13±0.14	2.13	1.7868	1.8155±0.0008	1.64
B7	6.43	6.50±0.12	1.09	1.7247	1.7548±0.0014	1.74
B8	4.70	4.56±0.11	3.00	1.6618	1.6909±0.0017	1.75
C	78.47	76.1±1.6	3.00	1.5997	1.612±0.002	0.74
D1	13.39	13±1	2.99	1.7005	1.728±0.006	1.61
D2	19.54	18.9±1.4	3.00	1.8026	1.836±0.011	1.87
D3	21.00	21.1±0.6	0.71	1.9039	1.928±0.005	1.27

D4	18.12	17.7±0.5	2.21	2.0046	1.995±0.010	0.48
D5	14.63	14.3±0.6	2.39	2.1048	2.078±0.009	1.23
D6	15.88	15.6±0.5	1.7	2.2070	2.239±0.006	1.42
D7	17.49	17.56±0.17	2.09	2.3085	2.322±0.006	0.60
E (TiO_2)	14.84	14.8±0.8	0.13	2.4096	2.389±0.010	0.87
F (SiO_2)	99.86	101.7±0.2	1.85	1.5003	1.5252±0.0011	1.64

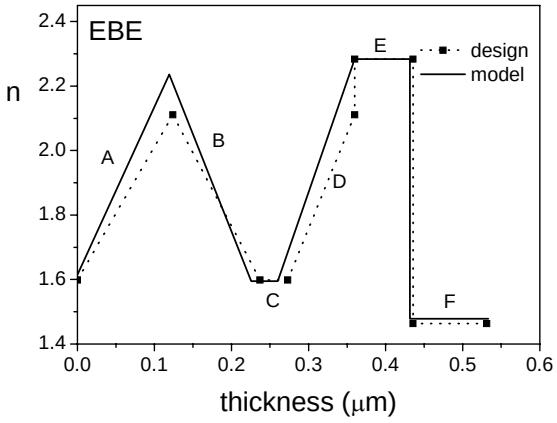
EBE
design
model
n
thickness (μm)
A
B
C
D
E
F

Fig. 1.a)

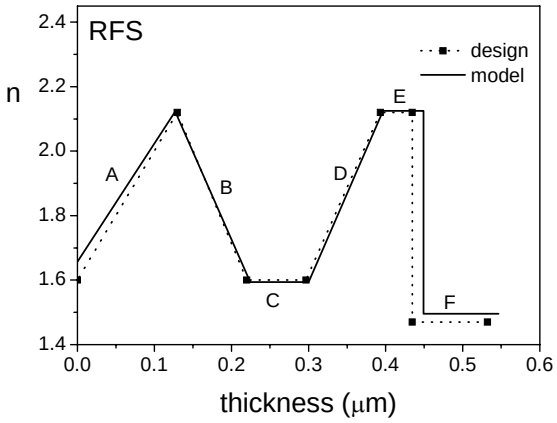
RFS
design
model
n
thickness (μm)
A
B
C
D
E
F

Fig. 1.b)

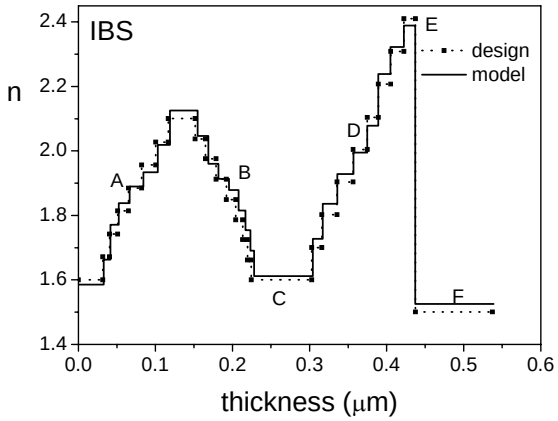
IBS
n
thickness (μm)
design
model
A
B
C
D
E
F
2.4
2.2
2.0
1.8
1.6
1.4
0.0
0.1
0.2
0.3
0.4
0.5
0.6

Fig. 1.c)

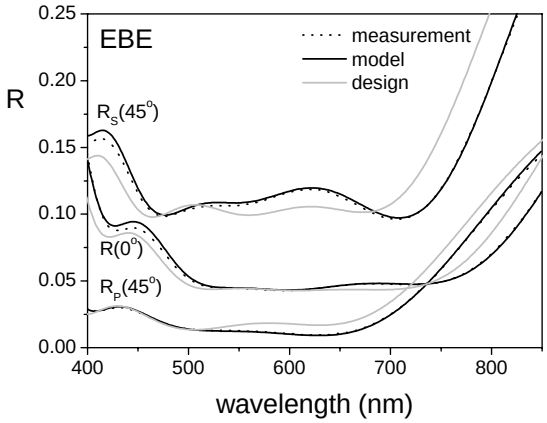
EBE
R
wavelength (nm)
measurement
model
design
R_S(45°)
R(0°)
R_P(45°)
0.25
0.20
0.15
0.10
0.05
0.00
400
500
600
700
800

Fig. 2.a)

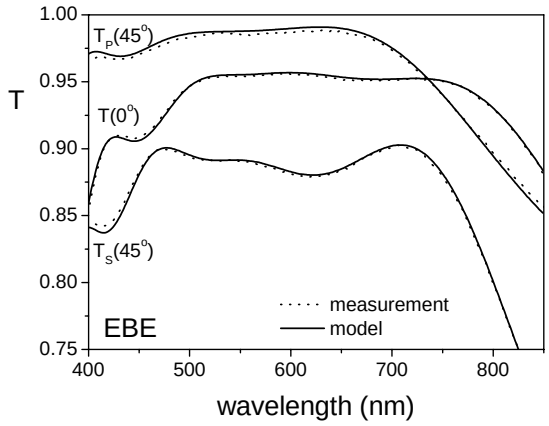
1.00
0.95
0.90
0.85
0.80
0.75
T
$T_P(45^o)$
$T(0^o)$
$T_S(45^o)$
EBE
measurement
model
400
500
600
700
800
wavelength (nm)

Fig. 2.b)

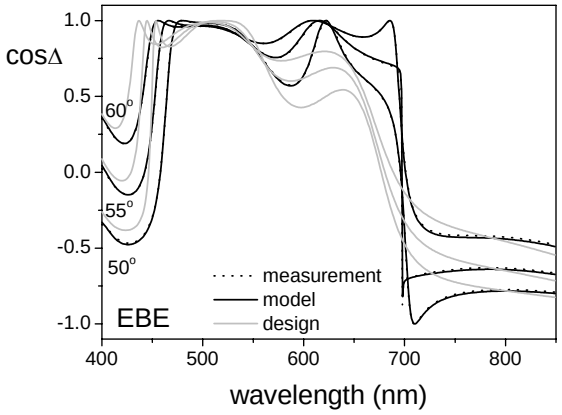
1.0
0.5
0.0
-0.5
-1.0
cosΔ
60^o
55^o
50^o
EBE
measurement
model
design
400
500
600
700
800
wavelength (nm)

Fig. 2.c)

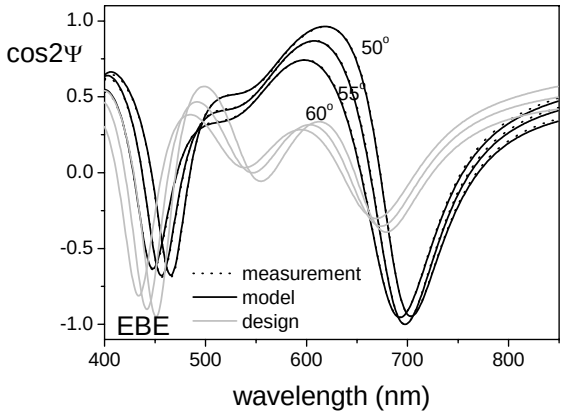
cos2Ψ
1.0
0.5
0.0
-0.5
-1.0
50°
55°
60°
measurement
model
design
EBE
400
500
600
700
800
wavelength (nm)

Fig. 2.d)

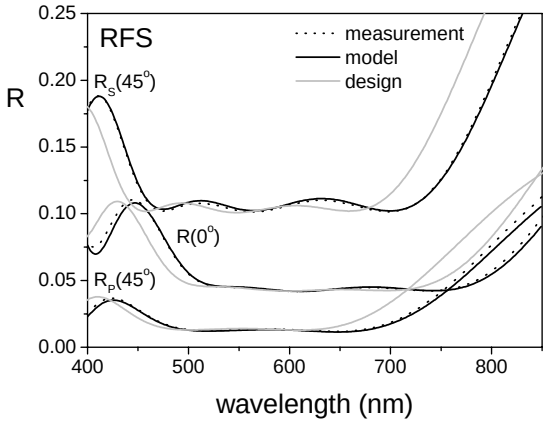
R
0.25
0.20
0.15
0.10
0.05
0.00
RFS
measurement
model
design
R_S(45°)
R(0°)
R_P(45°)
400
500
600
700
800
wavelength (nm)

Fig. 3.a)

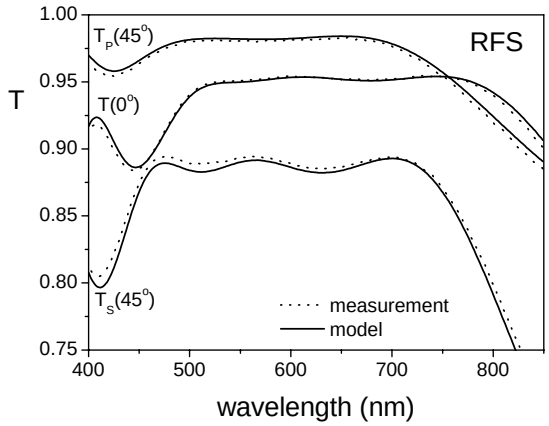
1.00
0.95
0.90
0.85
0.80
0.75
T
$T_P(45^o)$
$T(0^o)$
$T_S(45^o)$
RFS
measurement
model
400
500
600
700
800
wavelength (nm)

Fig. 3.b)

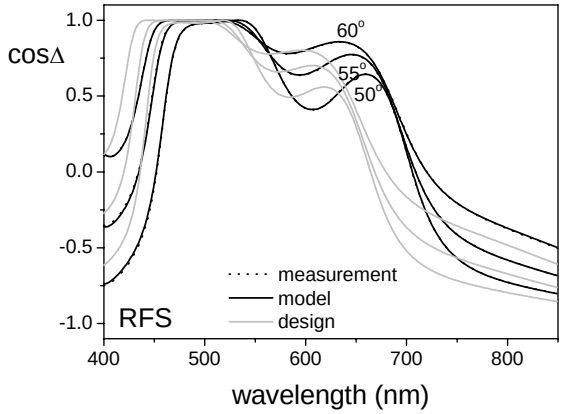
1.0
0.5
0.0
-0.5
-1.0
cosΔ
60^o
55^o
50^o
measurement
model
design
RFS
400
500
600
700
800
wavelength (nm)

Fig. 3.c)

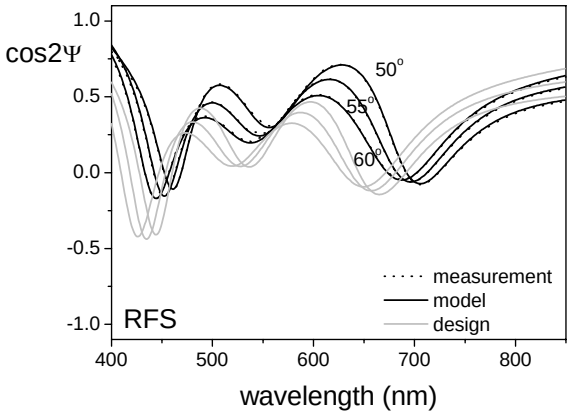
cos2Ψ
1.0
0.5
0.0
-0.5
-1.0
RFS
50°
55°
60°
measurement
model
design
400
500
600
700
800
wavelength (nm)

Fig. 3.d)

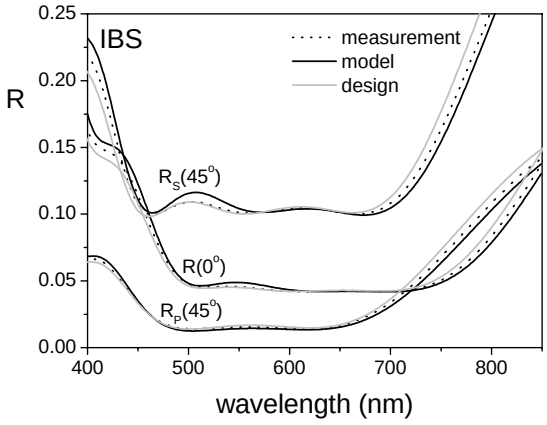
IBS
R
0.25
0.20
0.15
0.10
0.05
0.00
measurement
model
design
R_S(45°)
R(0°)
R_P(45°)
400
500
600
700
800
wavelength (nm)

Fig. 4.a)

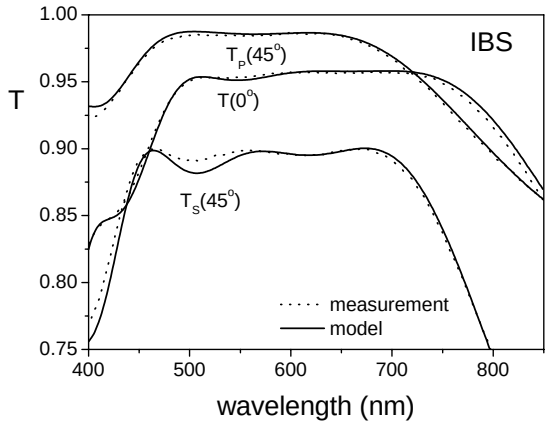
IBS
T
$T_P(45^o)$
$T(0^o)$
$T_S(45^o)$
measurement
model
wavelength (nm)

Fig. 4.b)

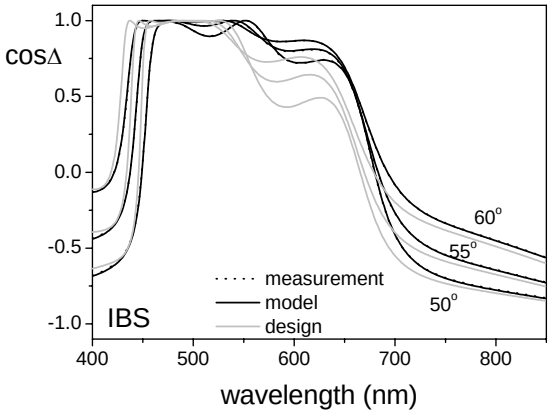
cosΔ
IBS
measurement
model
design
60^o
55^o
50^o
wavelength (nm)

Fig. 4.c)

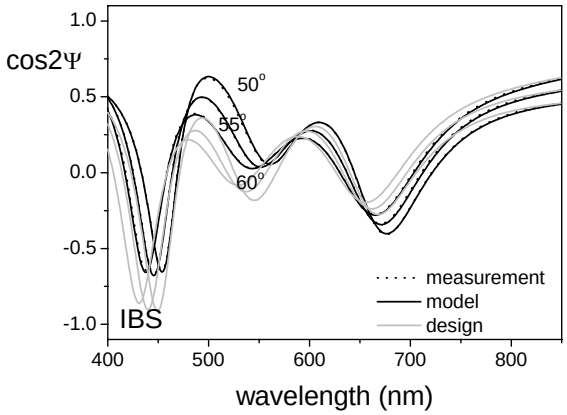
cos2Ψ
1.0
0.5
0.0
-0.5
-1.0
400
500
600
700
800
wavelength (nm)
50°
55°
60°
IBS
measurement
model
design

Fig. 4.d)